Chemical Engineering Journal 431 (2022) 134251

Contents lists available at ScienceDirect

Chemical Engineering Journal

journal homepage: www.elsevier.com/locate/cej

Dual-catalyst catalytic pyrolysis of poplar sawdust: A systematic study on first-layered catalysts

Xiangfei Xue [a,b], Changsen Zhang [c], Dan Xia [b], Yonggang Wang [d], Jie Liang [a,*], Yifei Sun [a]

[a] School of Energy and Power Engineering, Beihang University, Beijing 102206, China
[b] School of Space and Environment, Beihang University, Beijing 102206, China
[c] School of Ecology and Environment, Zhengzhou University, Zhengzhou, Henan 450001, China
[d] Center for High Pressure Science and Technology Advanced Research (HPSTAR), Beijing 100094, China

ARTICLE INFO

Keywords:
Dual-catalyst catalytic fast pyrolysis
Inorganic salts
Metal oxides
Porous materials
Bio-oil
Hydrocarbons

ABSTRACT

Dual-catalyst catalytic fast pyrolysis (CFP) technology is effective in converting biomass waste into hydrocarbon-rich bio-oils. However, systematic studies on dual-catalyst biomass CFP are limited, especially with respect to the best-performed dual catalyst design. In this context, dual-catalyst CFP of poplar sawdust was conducted with 18 *in-situ* first-layered catalysts, including 6 inorganic salts (NaCl, KCl, $MgCl_2$, $ZnCl_2$, K_3PO_4, and K_2HPO_4), 7 metal oxides (SiO_2, Al_2O_3, CaO, MgO, ZnO, Fe_2O_3, and CuO), and 5 porous materials (SBA-15, MCM-41, Y zeolite, Beta zeolite, and SAPO-34), while the ZSM-5 zeolite was fixed as an *ex-situ* second-layered catalyst. The effects of the 18 first-layered catalysts on bio-oil production were investigated and compared. Applying the porous materials as the first-layered catalysts increased the bio-oil yields compared to the inorganic salts and metal oxides. In particular, mesoporous SBA-15 combined with ZSM-5 led to the highest bio-oil yield of 19.4 wt% and a satisfactory hydrocarbon selectivity of 30.5 area%. The synergistic effects of the dual-layered catalysts were also studied. The first-layered catalysts cracked the primary biomass volatiles into smaller oxygenates, while the second-layered ZSM-5 deoxidized these molecules to hydrocarbons. In addition, the porous materials exhibited better synergy with ZSM-5 by simultaneously deoxygenating all the oxygenate types. The dual catalysts configured by Beta + ZSM-5 converted the most oxygenates into hydrocarbons, and the hydrocarbon selectivity (41.4 area%) was twice that in the blank experiment (*Thermal/ZSM-5*). Therefore, combining the porous materials and ZSM-5 delivers a promising catalyst for dual-catalyst biomass CFP.

1. Introduction

Biomass waste, such as forest and agricultural residues, has caused many harmful environmental problems because of their incineration leading to the direct release of toxic vapors (*e.g.*, NO_x, CO_x, polycyclic aromatic hydrocarbons) into the atmosphere [1]. However, as the only sustainable carbon resource, biomass waste can alternatively be converted into bioenergy, which could potentially solve environmental problems, and alleviate global energy pressures [2]. Among the various conversion methods, catalytic fast pyrolysis (CFP) technology is advantageous for bio-oil production owing to its simplicity and low cost [3]. Nevertheless, CFP technology is still in its development period and requires further modifications, with regards to either the equipment or catalyst, to improve the quality of the bio-oil produced [4,5].

In this context, the dual-catalyst CFP technology, which modified the traditional CFP by adding a second catalyst bed, was developed. Che *et al.* proved that the integrated *in-situ* pyrolysis of biomass using CaO (1st catalyst) and *ex-situ* upgrading using ZSM-5 (2nd catalyst) improved the hydrocarbon percentage in bio-oil [6]. Compared with traditional single-catalyst pyrolysis, dual-catalyst CFP technology combines the catalytic characteristics of the two catalysts in a sequential manner. For example, after the CaO catalyst cracks the large oxygenates in biomass vapors into smaller ones, the ZSM-5 catalyst subsequently catalyzes the conversion of smaller oxygenates into olefins and/or monocyclic aromatic hydrocarbons (MAHs). The dual-catalyst biomass CFP is also beneficial for enriching certain compounds during the pre-upgrading step, which improves the quality of the volatiles that pass through the second-layered catalyst [7]. Consequently, the deoxygenation capability of the second-layered catalyst, normally ZSM-5, is also strengthened [8]. There have been several pioneering works on dual-catalyst CPF;

* Corresponding author.
E-mail address: jieliang@buaa.edu.cn (J. Liang).

https://doi.org/10.1016/j.cej.2021.134251
Received 7 October 2021; Received in revised form 27 November 2021; Accepted 16 December 2021
Available online 21 December 2021

however, these were mainly concerned with the configuration of the metal oxides (*e.g.*, Al_2O_3, CuO, ZnO, and MgO) and ZSM-5 [5,8-11]. In addition to metal oxides, catalyst types such as inorganic salts or porous materials have been seldomly investigated as first-layered catalysts [12-14]. Therefore, to maximize the synergistic effect between dual catalysts and enhance hydrocarbon production, a systematic study on the combined catalyst design is imperative for dual-catalyst CFP technology.

As mentioned above, the catalyst plays a key role in biomass CFP, and most of the studied catalysts can be classified into inorganic salts, metal oxides, and porous materials [4,15]. Inorganic salts generally affect product distribution by altering the biomass decomposition route [4]. For example, NaCl suppresses levoglucosan production and prompts the cracking of rice husk into furans, alcohols, and phenols [16]. $MgCl_2$ and $ZnCl_2$ inhibits lignin degradation and increases the production of furfural and acetic acid [17,18]. K_3PO_4 prevents the decomposition of hemicellulose and increases phenol production [19]. Metal oxides have been demonstrated to effectively deoxidize biomass vapors and crack heavy molecules. For example, acidic Al_2O_3 preferentially expels oxygen from biomass vapors through a dehydration reaction [20]. Basic metal oxides (*e.g.*, CaO and MgO) actively catalyze ketonization reactions and hence promote the conversion of acids and ketones to hydrocarbons [6,21]. Transition metal oxides, such as CuO, Fe_2O_3, and ZnO facilitate the cracking of heavy matter in pyrolysis vapors and decrease the proportion of heavy fractions in bio-oil [22]. Finally, porous materials, are characterized by their deoxygenation capability, which benefits from the uniform channels and tunable acidic properties [23]. In particular, mesoporous silica (*e.g.*, MCM-41 and SBA-15) enable the cracking of heavy biomass oxygenates into light ones [15,24,25], and the zeolite catalysts (*e.g.*, Y, Beta, and ZSM-5) deoxygenated the biomass vapors *via* a series of catalytic reactions to yield hydrocarbons [26]. Among the porous catalysts, the ZSM-5 zeolite displayed the best deoxygenation capability owing to its strong Brönsted acidity and medium porosity, and has been extensively studied in biomass CFP [27]. Although the aforementioned catalysts are reportedly effective in improving the bio-oil quality, it is difficult to directly compare their catalytic performance because of the different biomass feedstocks and data formats used to describe the bio-oil quality [4]. Therefore, to determine the best-performing catalyst combination for dual-catalyst CFP, a batched pyrolysis of a fixed biomass feedstock with all three catalyst types is required.

As mentioned above, a detailed survey on the dual-catalyst CFP with more catalyst types (*e.g.*, inorganic salts, metal oxides, and porous materials) is required but currently limited. Herein, a systematic investigation of the dual-catalyst CFP of poplar sawdust was conducted in a fixed-bed reactor, which was configured by placing biomass + catalysts on the first layer and ZSM-5 on the second layer. In total, 18 catalysts, including six inorganic salts (NaCl, KCl, $MgCl_2$, $ZnCl_2$, K_3PO_4, and K_2HPO_4), seven metal oxides (SiO_2, Al_2O_3, CaO, MgO, ZnO, Fe_2O_3, and CuO), and five porous materials (SBA-15, MCM-41, Y, Beta, and SAPO-34) were separately studied as the first-layered catalysts. The pyrolysis product distribution and bio-oil composition were evaluated for each catalyst type. To determine the synergy between the dual-catalysts, we also conducted single-catalyst biomass CFP with the 18 catalysts, which further confirmed the advantage of the dual-catalyst mode.

2. Material and methods

2.1. Feedstock and catalysts

In this study, poplar sawdust, collected in Liaocheng, China, was used as the biomass feedstock. The feedstock was ground and sieved to less than 0.25 mm, and subsequently heated at 105 ℃ for 12 h prior to the pyrolysis experiments. The proximate and elemental composition of the poplar sawdust are listed in Table 1.

The catalysts used in this study were purchased from different manufacturers. Inorganic salts including NaCl and $MgCl_2·6H_2O$ were supplied by Tianjin Kemiou Chemical Reagent Co., Ltd.; $ZnCl_2$, K_3PO_4, and K_2HPO_4 were obtained from Shanghai Macklin Biochemical Co., Ltd.; and KCl was obtained from Luoyang Haohua Chemical Reagent Co., Ltd. For the metal oxides, SiO_2 was purchased from Beijing Xinxing Reagent Factory; Al_2O_3 was obtained from Sinopharm Chemical Reagent Co., Ltd; MgO was obtained from Tianjin Third Chemical Reagent Factory; CaO, CuO, and Fe_2O_3 were obtained from Shanghai Macklin Biochemical Co., Ltd.; and ZnO was from Shandong Ruiqi Chemical Co., Ltd. The porous materials including SBA-15 (Si/Al = ∞), MCM-41 (Si/Al = ∞), Y zeolite (Si/Al = 6), and Beta zeolite (Si/Al = 20) were supplied from Xianfeng Nano Co., Ltd; and SAPO-34 (Si/Al = 0.25) and ZSM-5 (Si/Al = 25) were obtained from the Nankai Catalyst Factory. Before pyrolysis, the metal oxides and porous materials were calcined at 550 ℃ for 4 h to remove moisture and impurities.

Table 1
Proximate and ultimate analysis of poplar sawdust.

Sample		Poplar sawdust
Proximate analysis[a] (wt.%)	Water	5.53
	Volatiles	78.23
	Fixed carbon	14.33
	Ash	1.91
	Total	100.00
Ultimate analysis[b] (wt.%)	C	46.53
	H	6.53
	O[c]	46.83
	N	0.11
	Total	100.00

[a] On air dry basis.
[b] On air dry ash-free basis.
[c] Calculated by difference.

2.2. Catalyst characterization

Powder X-ray diffraction (PXRD) measurements were carried out on a Bruker D8 diffractometer with a Cu Kα radiation source (40 mA, 40 kV). Scanning electron microscopy (SEM) images of the catalysts were obtained using a ZEISS Sigma 500 field emission scanning electron microscope operating at an accelerating voltage of 3 kV. Before observation, the samples were sprayed with gold for 30 s to improve their conductivity.

Temperature-programmed desorption of ammonia (NH_3-TPD) was performed using a chemical adsorption instrument (AutoChem II 2920). Before the experiment, the samples (200 mg) were pretreated with a helium stream at 500 ℃ for 3 h. Then, the temperature of the sample was cooled to 100 ℃. At this temperature, the sample adsorbed the ammonia mixture (10 vol% NH_3, 90 vol% He) to a saturated state. The samples were subsequently purged with a helium flow (30 mL/min) for 1 h until the chromatographic baseline flattened. Finally, the desorption experiment was conducted from 100 to 550 °C at a rate of 10 °C/min.

Temperature-programmed desorption of carbon dioxide (CO_2-TPD) was tested using an AutoChem II 2920 chemical adsorption instrument. Before the experiment, the samples (100 mg) were pretreated at 500 ℃ for 0.5 h and then cooled to 30 °C in a He atmosphere. The samples then adsorbed CO_2 to a saturated state in a mixed atmosphere of CO_2 (10 vol %) and He (90 vol%). In the desorption step, the saturated samples were immersed in a He flow (50 mL/min) for 1 h and heated from 100 to 900 °C at a heating rate of 10 °C/min.

Hydrogen temperature-programmed reduction (H_2-TPR) was performed on an AutoChem II 2920 chemical adsorption instrument from 50 to 900 °C at a heating rate of 10 °C /min. The samples (100 mg) were treated at 300 °C in argon for 8 h before reduction. During the test, a gaseous mixture containing 10 vol% H_2 and 90 vol% Ar was used to reduce the samples. The hydrogen consumption was monitored using a thermally conductive detector.

N_2 adsorption experiments were performed on a Quantachrome

Autosorb-iQ instrument at 77 K. Prior to adsorption, the samples were pretreated at 300 °C for 6 h under vacuum to remove the gas in the pores. The surface area of catalysts was calculated using the Brunauer-Emmett-Teller (BET) method. The pore size distribution of mesoporous materials (SBA-15 and MCM-41) and zeolites (Y zeolite, Beta zeolite, and SAPO-34) were measured using the Barrett-Joiner-Halenda (BJH) and the Non-Linear Density functional theory (NLDFT) method, respectively.

2.3. Catalytic pyrolysis experiments

The pyrolysis experiments were conducted in a fixed-bed reactor equipped with a quartz tube (length 50 cm, internal diameter 16 mm) and an infrared heating tube. A detailed description of the equipment has been reported in our previous work, and is depicted in **Fig. S1** [7]. A schematic diagram of the single- and dual-catalyst CFP configurations are shown in Fig. 1. In the single-catalyst CFP experiment (Fig. 1**a**), a well-mixed biomass (1.0 g) and first-layered catalyst (0.5 g) was packed in the middle of the quartz tube, and the two ends were fixed with quartz wool. Before pyrolysis, a nitrogen gas flow was purged into the system at a rate of 200 mL/min for 30 min. Then, the system was heated rapidly to 500 ℃ within 50 s and maintained for another 5 min to release as much volatiles as possible. Meanwhile, the volatiles were driven to the condenser tubes using nitrogen at a flow rate of 100 mL/min. The two consecutive condensers were fully immersed in ice water (~0 ℃), wherein condensable volatiles were collected as liquid, and non-condensable volatiles were collected as gas in bags. For the dual-catalyst CFP experiments (Fig. 1**b**), a second catalyst layer of ZSM-5 (1.0 g) was added at the end of the first catalyst layer, while all other reaction conditions remained the same. Notably, the dual-catalyst CFP was a combined system that consecutively integrated the *in-situ* pyrolysis of biomass (for the first-layer catalyst) and *ex-situ* pyrolysis mode (for the second catalyst). All pyrolysis experiments were conducted at least twice for data repeatability.

The pyrolysis products were categorized into three classes: solid, liquid, and gas products. The solid product was composed of char and coke, and their total weight was calculated by subtracting the mass of the catalyst from the mass of the remaining solid in the quartz tube. The liquid product was a mixture of water and bio-oil, and its total weight was calculated by the mass difference of the condensers before and after the reaction. After extraction with dichloromethane, the water phase floated to the upper layer, whereas the bio-oil phase dissolved in dichloromethane and sank to the lower layer. Therefore, the water and bio-oil phases were collected and weighed separately. Based on the conservation of mass, the weight of the gas product is equal to the initial mass of the biomass minus that of the solid and liquid. The detailed equations are as follows:

$$Y_{solid} = \frac{M_{solid\ \ residue} - M_{catalyst} - M_{quartz\ wool}}{M_{biomass}} \times 100\% \tag{1}$$

$$Y_{liquid} = \frac{M_{condenser+liquid} - M_{condenser}}{M_{biomass}} \times 100\% \tag{2}$$

$$Y_{gas} = 100\% - Y_{solid} - Y_{liquid} \tag{3}$$

$$Y_{water} = \frac{M_{water}}{M_{biomass}} \times 100\% \tag{4}$$

$$Y_{bio-oil} = Y_{liquid} - Y_{water} \tag{5}$$

where $M_{biomass}$ denotes the mass of dry biomass; $M_{solid\ residue}$ represents the total mass of solid left in the quartz tube; $M_{catalyst}$ refers to the initial mass of the first-layer and second-layer catalysts; $M_{quartz\ wool}$ denotes the mass of quartz wool; $M_{condenser}$ and $M_{condenser+liquid}$ represent the mass of the condensers before and after pyrolysis, respectively; and M_{water} is the mass of the water phase.

2.4. Characterization of the bio-oil and gas

The chemical composition of the bio-oil was analyzed using gas chromatography/mass spectrometry (GC/MS, Shimadzu QP2010 Ultra) coupled with an RXI-5SiL-MS capillary column (30.0 m × 0.25 mm × 0.25 μm). The temperature program of the GC was initiated at 50 ℃ for 3 min and raised to 200 ℃ at a heating rate of 8 ℃/s. Then, the temperature was raised to 280 ℃ within 2 min, and finally maintained for another 5 min. The injector temperature was 250 ℃, and the injection size was 1.0 μL with a split ratio of 20:1. The carrier gas was high-purity helium with a flow rate of 1.0 mL/min. For the mass spectrometer, the ion source temperature and interface temperature were set at 200 ℃ and 250 ℃, respectively. The NIST11 (National Institute of Standards and Technology) mass spectral library was used to identify the compounds in the bio-oil, and the peak area percentage was used to evaluate the variation of organics [28]. The gas products were analyzed by GC (GC-7920, Zhongjiao Jinyuan, China) with a thermal conductivity detector (TCD) (column: TDX-01, 3 mm × 3 m). The oven temperature was maintained at 80 ℃. The inlet temperature and TCD temperature were set to 100 ℃. To ensure reproducibility, each experiment was performed at least twice and the relative standard deviation for the gases was less than 10%.

3. Results and discussion

3.1. Catalyst characterization

The PXRD patterns of all the catalysts were summarized in **Fig. S2**.

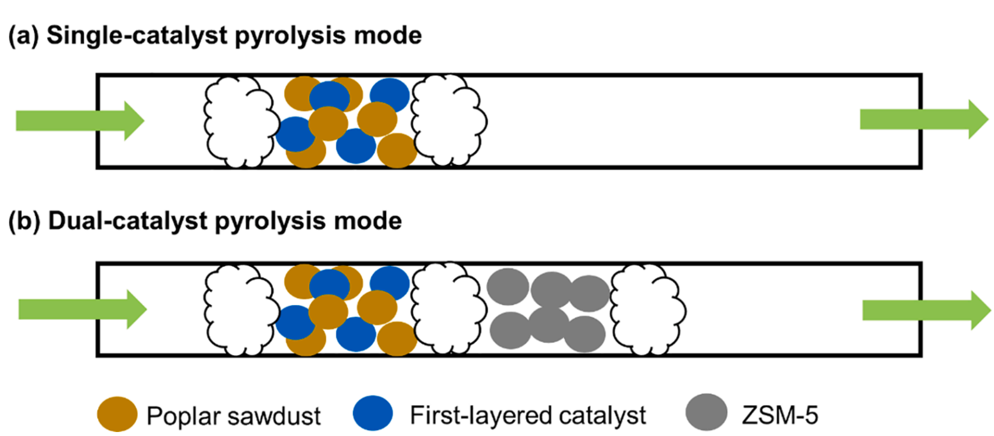

Fig. 1. Schematic diagram of the single-catalyst and dual-catalyst CFP modes.

The strong peak intensity and narrow width suggest they all possess high crystallinity (except Al_2O_3). Each powder pattern was consistent with its standard PDF card, indicating a high phase purity for most catalysts. The discrepancy between the peak of K_2HPO_4 and K_3PO_4 was attributed to their easy deliquescence, which can be evidenced from their SEM images (**Fig. S3**). The characteristic peaks of the inorganic materials (**Fig. S2a**) and metal oxides (**Fig. S2b**) were distributed in a higher 2θ range (10–50°) than those for porous materials (2θ = 5–30°, **Fig. S2c-d**), which is consistent with the abundant internal channels in zeolites and mesoporous silica. In addition, mesoporous silica with the largest pore size exhibited the lowest peak position (2θ = 0.7–2°).

The SEM images of all the catalysts are depicted in **Fig. S3-S5**. For inorganic salts (**Fig. S3**), NaCl and KCl exhibited an irregular bulky morphology (~6 μm), whereas K_2HPO_4 accumulated crystals less than 0.5 μm. **Fig. S4** shows SEM images of the metal oxides, which also exhibited irregular morphologies. Although SiO_2 and Al_2O_3 had bulky crystals of > 100 μm and ~ 20 μm, respectively, the other metal oxides (CaO, CuO, ZnO, and Fe_2O_3) had smaller particle sizes of 0.3–2 μm. The MgO catalyst possessed a layered stacking morphology, dotted with small particles (~300 nm). SEM images of the porous materials are summarized in **Fig. S5**. SBA-15 had a worm-like morphology with a length of ~ 1 μm, whereas MCM-41 and Y had rod-like crystals of ~ 500 nm and ~ 1 μm, respectively. In addition, although Beta was loosely nanoparticles, SAPO-34 exhibited a well-defined cubic crystal with a large size > 2 μm.

The acidity of the catalysts was analyzed using NH_3-TPD (**Fig. S6** and Table 2). Generally, the intensity and position of the ammonia desorption peak are directly related to the number and strength of acidity, respectively [29]. With regards to metal oxides, SiO_2 had no prominent ammonia desorption peak, indicative of an extremely weak acidity. For comparison, Al_2O_3 showed two desorption peaks at 176.9 and 383.6 ℃, suggesting the presence of weak and strong acid sites with a total acidity of 0.25 mmol/g. Regarding porous materials, the mesoporous silica (SBA-15 and MCM-41) were weakly acidic owing to the absence of Al. In contrast, the aluminosilicate zeolites (Y, SAPO-34 and Beta) were strongly acidic with total acidities of 1.680, 1.375, and 0.615 mmol/g, respectively.

The alkalinity of CaO, MgO and K_3PO_4 was analyzed by CO_2-TPD curves (**Fig. S7**). The higher temperatures and greater amount of CO_2 desorption suggested an increased number of stronger alkalinity, respectively [30]. As shown, CaO exhibited an intense peak located at 709.4 ℃ with a total CO_2 consumption of 1.459 mmol/g. This value was much higher than that for MgO (0.097 mmol/g) and K_3PO_4 (0.102 mmol/g), suggesting a stronger alkalinity for CaO.

The reducibility of the transition metal oxides was evaluated using H_2-TPR. The peak intensity and position of H_2 desorption were directly related to the amount and strength of reducibility, respectively [31]. As shown in **Fig. S8**, ZnO showed no reduction peak in the entire temperature range (100–900 ℃), indicating its poor reducibility. Fe_2O_3 exhibited a reduction peak at 402.9 ℃, followed by a broad band centered at 564.6 and 721.6 ℃, respectively, corresponding to the reduction of $Fe_2O_3 \rightarrow Fe_3O_4 \rightarrow Fe$ [32]. For CuO, hydrogen consumption began at 210 °C and the reduction peak was centered at 346.4 ℃, owing to the reduction of CuO to metallic Cu (Table S1) [33]. The reduction temperature for CuO was much lower than that for Fe_2O_3 due to the weak Cu–O bond, providing it with a better oxygen supply capacity.

The textural properties of the porous materials were characterized using N_2 sorption experiments (**Fig. S9**). Among them, SBA-15 and MCM-41 exhibited a hysteresis loop in the P/P_0 range of 0.7–0.85 and 0.3–0.4, respectively, confirming the presence of mesopores. The higher loop range in SBA-15 also indicates its larger pore size, as shown in **Fig. S9b**. In contrast, all microporous materials (Y, SAPO-34 and Beta zeolites) demonstrated a type I sorption isotherm with rapid N_2 adsorption in the range of P/P_0 less than 0.001. In contrast to the saturated platforms in Y and SAPO-34, the adsorption isotherm for Beta further increased at P/P_0 > 0.55 and a hysteresis loop was observed in the desorption branch, indicating the presence of intra-crystal mesopores (6.40, 8.63 nm) (**Fig. S9c**), which was consistent with the SEM image (**Fig. S5**). Table 3 summarizes the surface area, pore volume, and pore size of the materials. The pore diameter clearly decreased in the order of SBA-15 (8.15 nm) > MCM-41 (2.70 nm) > Y zeolite (7.4 Å) > Beta zeolite (6.7 Å) > SAPO-34 (4.3 Å).

3.2. Dual-catalyst CFP using different first-layer catalysts

In the dual-catalyst CFP of poplar sawdust, ZSM-5 was fixed as the second-layered catalyst, while the *in-situ* first-layered catalyst was studied using six inorganic salts (NaCl, KCl, $MgCl_2$, $ZnCl_2$, K_3PO_4, and K_2HPO_4), seven metal oxides (SiO_2, Al_2O_3, CaO, MgO, ZnO, Fe_2O_3, and CuO), and five porous materials (SBA-15, MCM-41, Y, Beta, and SAPO-34). The effects of the first-layered catalysts on bio-oil production are summarized in this section. For comparison, *ex-situ* CFP over ZSM-5 (denoted as *thermal/ZSM-5*) was performed as a blank experiment.

3.2.1. Effect of inorganic salts on the dual-catalyst CFP of poplar sawdust

Inorganic salts, including two neutral salts (NaCl and KCl), two acidic salts ($MgCl_2$ and $ZnCl_2$), and two basic salts (K_3PO_4 and K_2HPO_4), were initially studied as first-layered catalysts, and their effects on bio-oil production are depicted in Fig. 2. Compared to the blank experiment, the addition of inorganic salts decreased the bio-oil yield but increased that of water (Fig. 2**a**), which confirmed a favored dehydration route for this catalyst type. The variation trend was even larger for acidic salts, and the $MgCl_2$ catalyst produced the highest water (44.4 wt%) and the lowest bio-oil yield (12.3 wt%). The solid yield was dependent on the acid-base properties of the first-layered catalysts. Although it decreased for basic (K_3PO_4 and K_2HPO_4) and acidic salts ($MgCl_2$), it increased for neutral salts (NaCl and KCl) compared to that in the blank experiment. However, the maximum solid yield (19.9 wt%) was achieved by $ZnCl_2$ with a transition metal. This is because, compared to the ionic bonds in other salts, the partial co-valent nature of Zn^{2+} weakened the bonding interaction with the active oxygenated intermediates and was thus unable to hinder their repolymerization to coke [34]. The $ZnCl_2$ catalyst also exhibited a minimum gas yield (22.4 wt%) owing to its inhibition of lignin devolatilization and holocellulose (cellulose and hemicellulose) ring scission [18].

The chemicals detected by GC–MS in bio-oil can be classified into acids, aldehydes, ketones, hydrocarbons, and phenols based on their organic functional groups. Their relative selectivity was dependent on the acidity and basicity of the first-layered catalysts (Fig. 2**b**). Compared

Table 2
Acid amount of the two metal oxides and porous material catalysts.

Catalysts	Peak 1 (℃)	Quantity (mmol/g)	Peak 2 (℃)	Quantity (mmol/g)	Total amount (mmol/g)
SiO_2	–	–	–	–	–
Al_2O_3	176.9	0.156	383.6	0.094	0.250
SBA-15	–	–	416.3	0.030	0.030
MCM-41	141.2	0.020	304.5	0.032	0.052
Y zeolite	160.5	0.89	205.4	0.79	1.680
Beta zeolite	189.8	0.471	374.4	0.144	0.615
SAPO-34	168.8	0.703	382.3	0.672	1.375

Table 3
Textural properties of the different porous material catalysts.

Catalysts	BET area(m^2/g)	Pore volume (cm^3/g)	Pore size(nm)
SBA-15	497.8	1.27	8.15
MCM-41	1092.2	0.98	2.70
Y zeolite	795.1	0.37	0.74
Beta zeolite	580.8	0.48	0.67 (6.40, 8.63)
SAPO-34	631.0	0.28	0.43

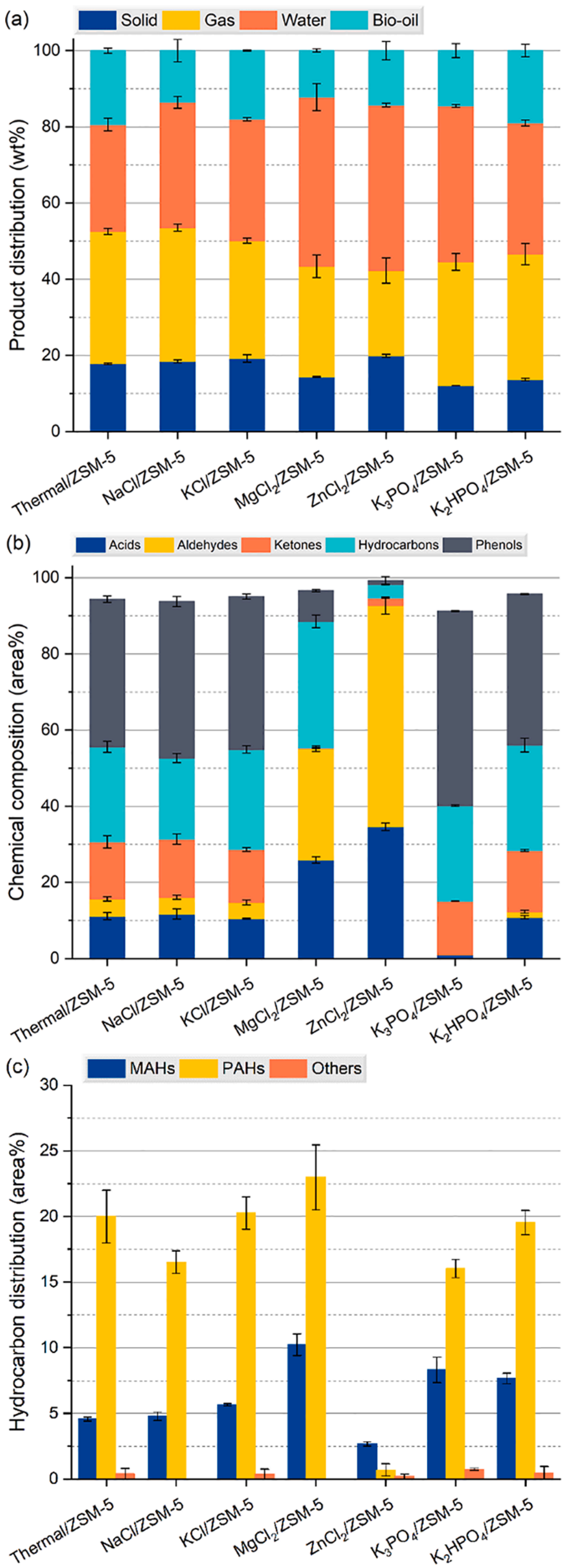

Fig. 2. Effect of inorganic salts on the (a) product distribution, (b) bio-oil composition, and (c) hydrocarbon production.

to the blank experiment, the addition of neutral salts (NaCl and KCl) barely changed the bio-oil composition. In contrast, the addition of acidic salts ($MgCl_2$ and $ZnCl_2$) dramatically increased the selectivity of acids and aldehydes while decreasing that of ketones and phenols. Notably, the Lewis acidic $ZnCl_2$ exhibited the highest selectivity for acids (34.6 area%) and aldehydes (58.1 area%), which was ~ 3 and ~ 13 times that for *thermal/ZSM-5*, respectively. This is consistent with previous reports that $ZnCl_2$ favors the formation of acetic acids and furfural by enhancing the depolymerization and dehydration of holocellulose [18]. Although the acidic $MgCl_2$ yielded less acids (25.9 area %) and aldehydes (29.3 area%) than $ZnCl_2$, it achieved a maximum selectivity of hydrocarbons (33.2 area%) and especially MAHs (10.2 area%) (Fig. 2**c**). This could be attributed to the ionic nature of Mg^{2+}, which bound more fragments of oxygenated intermediates and improved the quality of biomass vapors that go through second-layered catalysts [35]. The basic salts (K_3PO_4 and K_2HPO_4) decreased the selectivity for acids and aldehydes; however, this increased the selectivity for phenols. In particular, K_3PO_4 performed better in producing phenols (51.0 area%) and suppressing acids (1.0 area%) than K_2HPO_4 (39.7 and 10.8 area%) (Fig. 2**b**). This is because K_3PO_4 is better promoting lignin decomposition and inhibition holocellulose decomposition, owing to its higher alkalinity [19]. In addition, although K_3PO_4 decreased the hydrocarbon selectivity compared to K_2HPO_4, it yielded more MAHs (8.3 *vs.* 7.7 area%) owing to its superior cracking capability (Fig. 2**c**).

The composition of the gaseous products are listed in Table 4. In the blank experiment (*Thermal/ZSM-5*), CO_2 (41.9 vol%) and CO (39.8 vol %) were the dominant gas components, followed by H_2 (6.7 vol%) and CH_4 (11.6 vol%). The formation of carbon oxides is related to the cracking of the C-O structures in holocellulose. H_2 was formed from C-H or O–H bond cleavage or from the condensation of aromatic structures. CH_4 was presumably obtained from the reaction between hydrogen and the methyl free radicals, which dissociated from the side chains of the aromatic rings in lignin. Notably, the addition of KCl barely changed the gas composition, as it did in the bio-oil composition. However, the other neutral (NaCl) and acidic salts ($MgCl_2$ and $ZnCl_2$) dramatically increased the CO_2 proportion to 62.7–65.9 vol%, while decreasing that for CO to 11.5–26.4 vol%. The H_2 and CH_4 proportions also decreased for NaCl and $MgCl_2$. This was attributed to a favored decarboxylation reaction during holocellulose pyrolysis and suppressed lignin decomposition [36], consistent with the bio-oil analysis results. In contrast, the H_2 fraction for $ZnCl_2$ increased 2.5 times compared to that for the blank experiment, indicating a preferred water–gas shift reaction ($CO + H_2O = H_2 + CO_2$). Although the basic salts (K_3PO_4 and K_2HPO_4) also changed

Table 4
The mean volumetric percentages (%) of gas compounds produced from the dual-catalyst pyrolysis of poplar sawdust.

Catalyst	CO_2	CO	H_2	CH_4
Thermal/ZSM-5	41.9	39.8	6.7	11.6
NaCl/ZSM-5	62.7	26.4	3.1	7.8
KCl/ZSM-5	40.4	42.8	4.6	12.2
$MgCl_2$/ZSM-5	65.9	21.9	5.7	6.6
$ZnCl_2$/ZSM-5	64.4	11.5	21.4	2.7
K_3PO_4/ZSM-5	37.4	31.0	18.7	12.8
K_2HPO_4/ZSM-5	39.1	44.3	4.3	12.3
SiO_2/ZSM-5	34.7	44.8	7.1	13.5
Al_2O_3/ZSM-5	29.1	49.1	7.6	14.2
CaO/ZSM-5	33.6	31.1	21.4	14.0
MgO/ZSM-5	50.6	38.4	2.2	8.8
ZnO /ZSM-5	40.9	38.0	12.1	8.9
CuO /ZSM-5	32.9	41.6	18.9	6.6
Fe_2O_3 /ZSM-5	42.7	32.9	15.6	8.8
SBA-15/ZSM-5	54.7	35.2	1.4	8.8
MCM-41/ZSM-5	43.2	44.7	2.7	9.4
Y zeolite/ZSM-5	42.4	44.4	2.3	10.9
Beta zeolite/ZSM-5	42.2	48.7	1.5	7.6
SAPO-34/ZSM-5	34.5	51.3	4.2	10.0

the gas composition, K_3PO_4 dramatically increased the H_2 fraction by two times, consistent with its promotion of lignin decomposition.

In summary, although the application of inorganic salts as first-layered catalysts decreased the bio-oil yield, they helped to enrich certain compounds in the pre-upgrading step. In particular, acidic $ZnCl_2$ and $MgCl_2$ favored the formation of furfural and acetic acids, and basic K_3PO_4 promoted the enrichment of phenols in bio-oil.

3.2.2. Effect of metal oxides on the dual-catalyst CFP of poplar sawdust

In this section, two acidic metal oxides (SiO_2 and Al_2O_3), two basic metal oxides (MgO and CaO), and three transition metal oxides (ZnO, CuO, and Fe_2O_3) were investigated as *in-situ* first-layered catalysts, and their effects on bio-oil production are summarized in Fig. 3. Similar to inorganic salts, the addition of metal oxides decreased the bio-oil yield while increasing that of water (Fig. 3**a**) compared to that in the blank experiment. The acidic Al_2O_3 led to the highest water yield (38.7 wt%) owing to its strong dehydration capability. The solid yield variation trend depended on the acidic/basic properties of metal oxides; that is, while the acidic metal oxides (SiO_2 and Al_2O_3) slightly decreased the solid yield from 17.9 wt% in *Thermal/ZSM-5* to 16.3–17.2 wt%, the basic metal oxides (MgO and CaO) increased the value to 21.7–21.9 wt%. The higher solid yield of basic metal oxides may be due to their reaction with non-condensable gases (*e.g.*, CO_2) and organic acids to form $CaCO_3$, $MgCO_3$, and organic calcium/magnesium salts [37]. The gas yield decreased for both acidic and basic metal oxides, while increasing for transition metal oxides (CuO and Fe_2O_3) with oxidation and reduction properties. This is attributed to the oxygen species in transition metal oxides, which can be released into the biomass vapors under a reduction atmosphere and participate in the cracking of heavy molecules (*e.g.*, tar) into gases [33]. Therefore, these transition metal oxides can be viewed as oxidative catalysts. Because the oxygen species in CuO is more active than that in Fe_2O_3 (Table S1), the CuO catalyst led to a higher gas yield (38.4 wt%) and a lower solid yield (12.9 wt%).

The effect of metal oxides on the chemical composition of bio-oil produced from dual-catalyst biomass CFP are shown in Fig. 3**b**. Compared to the blank experiment, applying acidic metal oxides (SiO_2 and Al_2O_3) as first-layered catalysts only slightly altered the bio-oil composition, although the more acidic Al_2O_3 had a greater impact in reducing the selectivity of phenols (34.9 *vs.* 37.4 area%) and ketones (12.7 *vs.* 19.3 area%), in addition to increasing that for hydrocarbons (29.4 *vs.* 24.4 area%) and MAHs (6.4 *vs.* 5.9 area%) (Fig. 3**c**). This is consistent with previous reports that Al_2O_3 effectively reduces the oxygen content of bio-oil through a dehydration reaction [38]. The basic metal oxides (CaO and MgO) also only slightly affected the bio-oil composition; however, the variation trend is different from that in acidic metal oxides. For example, the CaO and MgO catalysts slightly increased the phenols selectivity from 38.7 area% in *Thermal/ZSM-5* to 43.6–45.3 area%, but decreased the hydrocarbon selectivity from 25.0 area% to 20.4–21.7 area%. Given that phenols are mainly derived from lignin degradation, the increased phenol selectivity may be attributed to poor holocellulose degradation in the presence of alkaline metal oxides [39]. By catalyzing the ketonization of carboxylic acids and/or aldehydes, the strongly alkaline CaO catalyst also decreased the selectivity of acids and aldehyde by half (2.0 and 4.9 area% *vs.* 4.5 and 11.1 area%, respectively), while increasing that for ketones (15.0 *vs.* 21.7 area%) compared to that in *Thermal/ZSM-5* [40]. The weakly alkaline metal oxide MgO (**Fig. S7**) effected the production of acids, aldehydes, and ketones less than CaO, although it increased the MAHs selectivity from 4.6 area% in *Thermal/ZSM-5* to 7.5 area% (Fig. 3**c**) [21]. The effect of transition metal oxides on the bio-oil composition is dependent on the metal type. For example, the ZnO catalyst barely changed the bio-oil composition, whereas CuO and Fe_2O_3 clearly inhibited the production of hydrocarbons by promoting phenols, ketones, and acids (Fig. 3**b-c**). This is attributed to the high activity of CuO and Fe_2O_3 for decomposing lignin and hemicellulose, as previously observed [41]. The difference between CuO and Fe_2O_3 lies in the aldehyde content; that is, while CuO

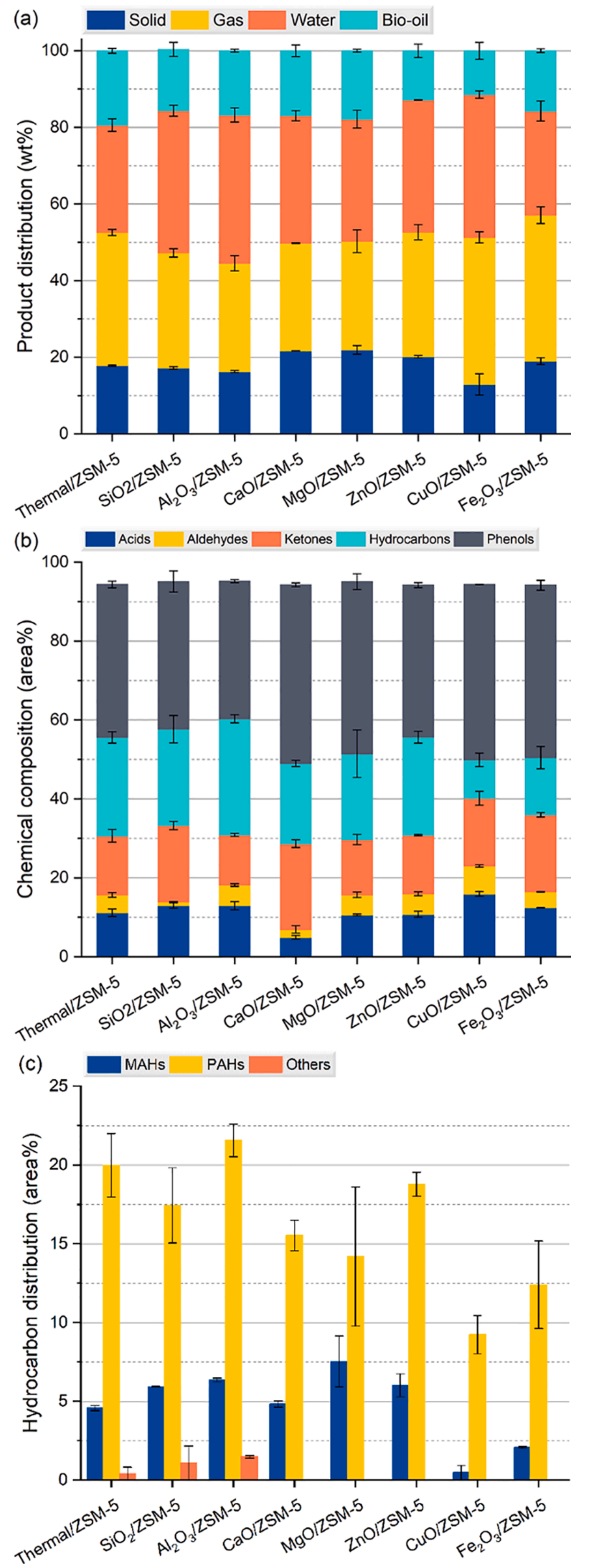

Fig. 3. Effect of metal oxides on the (a) product distribution, (b) bio-oil composition, and (c) hydrocarbon production.

promoted the production of aldehydes, Fe_2O_3 decreased the aldehyde selectivity. This is due to aldehydes being more reactive than ketones toward polymerization [42], and their evolution is affected more by the oxygen vacancies in the transition metal oxides [41].

The gas composition also varied with metal oxides. Compared to *Thermal/ZSM-5*, adding acidic metal oxides (SiO_2 and Al_2O_3) notably increased the CO selectivity from 39.8 to 44.8–49.1 vol%, while decreasing the CO_2 selectivity from 41.9 to 29.1–34.7 vol%. This is due to the favored Boudouard reaction ($C + CO_2 = 2CO$) between tar and CO_2 [43], which is consistent with the reduced solid yield by acidic metal oxides (Fig. 3**a**). Alkaline metal oxides (CaO and MgO) showed opposite selectivity variations toward CO_2, H_2, and CH_4. In particular, the more basic CaO notably increased the H_2 and CH_4 proportion to 21.3 and 14.0 vol%, respectively, while decreasing the CO_2 fraction to 33.6 vol% owing to the reaction between CO_2 and CaO forming $CaCO_3$. The increased proportion of H_2 and CH_4 was attributed to the enhanced lignin degradation by CaO, which was also consistent with the increased phenol fraction in bio-oil. In contrast, the less basic MgO decreased the fraction of H_2 and CH_4, while increasing that for CO_2, indicating a preferred decarboxylation reaction. Regarding the transition metal oxides (ZnO, CuO and Fe_2O_3), they all decreased the CH_4 fraction (11.6 → 6.6–8.9 vol%), while increasing that for H_2 (6.7 → 12.1–18.9 vol%) compared to the blank experiment. This was attributed to a partial reaction between methane and the oxygen released from transition metal oxides, forming of H_2 and CO [44,45]. In particular, CuO with a better oxygen supply capacity, led to the highest H_2 fraction (18.9 vol%) and lowest CH_4 fraction (6.6 vol%). Notably, Fe_2O_3 further decreased the CO selectivity (32.9 vol%) by increasing that for CO_2 (42.7 vol%), owing to its positive effect on the water–gas shift reaction ($CO + H_2O = H_2 + CO_2$) [46].

As mentioned above, the application of metal oxides as first-layered catalysts not only reduced the bio-oil yield, but also suppressed the hydrocarbon production (except for Al_2O_3). Nevertheless, some improved the quality of biomass volatiles by decreasing the heavy molecule fraction or by enriching the high-value compounds. In particular, the basic CaO inhibited the production of acids and enhanced that of phenols, and the transition metal oxides (CuO and Fe_2O_3) with multiple valences led to higher amounts of phenols, acids and ketones.

3.2.3. Effect of porous materials/ZSM-5 on the pyrolysis product

Five porous materials, including two mesoporous silica (SBA-15 and MCM-41) and three zeolites (Y, Beta, and SAPO-34) were tested as first-layered catalysts in this section, and their effects on the bio-oil production are depicted in Fig. 4. Interestingly, the addition of porous materials only slightly decreased the bio-oil yield by 0–23 % (Fig. 4**a**) compared to that in the blank experiment (19.4 wt%). The mesoporous SBA-15 barely reduced the bio-oil yield of 19.4 wt%, owing to its large pore size and poor acidity [47]. In comparison, the three zeolites (Y, Beta, and SAPO-34) slightly lowered the bio-oil yield (15.0–18.7 wt%). This is attributed to the stronger acidity of zeolites, which is effective in catalyzing dehydration reactions and promoting water formation at a higher water yield. The gas yield decreased for all the porous catalysts (24.6–29.6 wt%) compared to that in blank experiment (34.7 wt%). The solid yield also decreased for all the porous materials (13.1–17.8 *vs.* 17.9 wt% in blank experiment) except for MCM-41. This, in addition to the relatively high bio-oil yield, suggests that the porous materials are promising first-layered catalyst candidates for bio-oil production.

The effect of porous materials on the bio-oil composition distribution are depicted in Fig. 4**b**, indicating that the porous materials are excellent catalysts for deoxidizing bio-oils. Compared to the blank experiment, all the porous materials (except SAPO-34) tended to increase the selectivity of hydrocarbons (26.8–41.1 *vs.* 25.0 area%), and especially that of MAHs (7.0–8.2 *vs.* 4.6 area%) (Fig. 4**c**). In addition, the application of large-pore zeolites (Beta and Y) as first-layered catalysts led to a higher hydrocarbon selectivity than mesoporous silica (MCM-41 and SBA-15). This is attributed to the presence of strong Brönsted acidic sites in

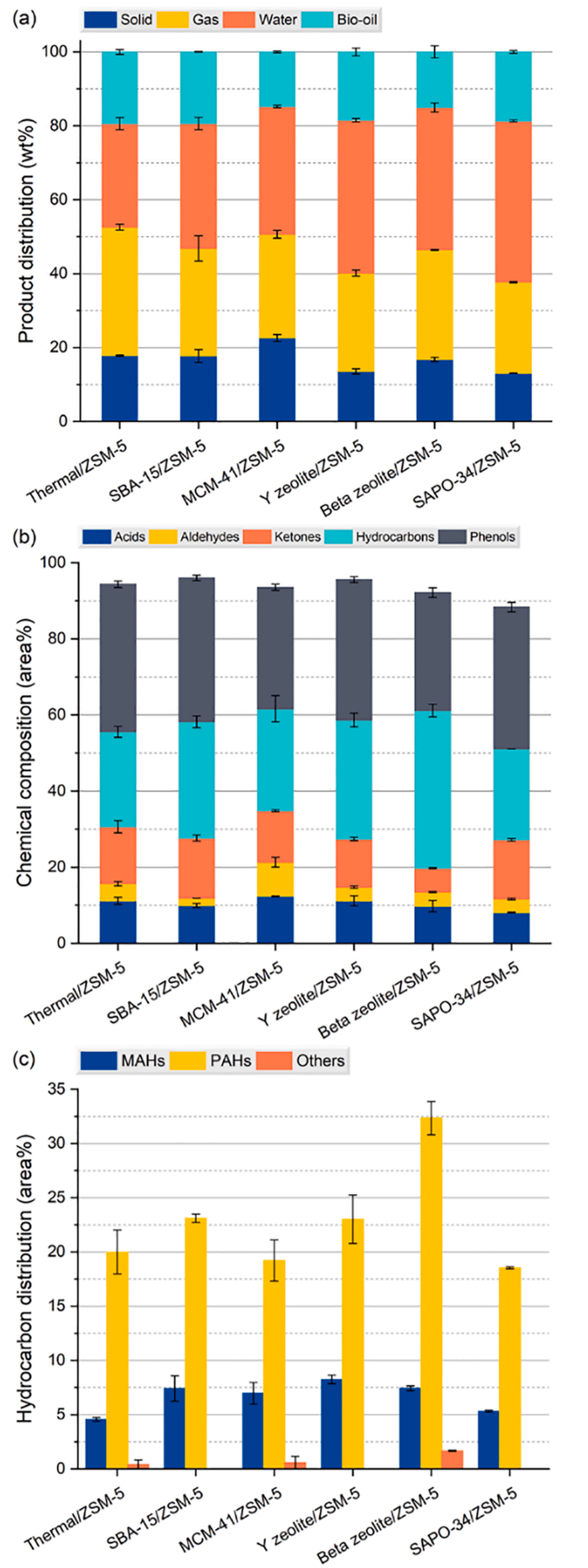

Fig. 4. Effect of porous materials on the (a) product distribution, (b) bio-oil composition, and (c) hydrocarbon production.

zeolites, which are needed to crack the oxygenated intermediates into hydrocarbons [48]. Given that a small-pore zeolite SAPO-34 decreased the hydrocarbon selectivity to 23.9 area%, a large pore size presumably also plays a role in the deoxygenation reactions by allowing the diffusion of large oxygenated-intermediates and access to inner Brönsted acid sites. Therefore, Beta zeolite with a large pore size and stacked mesopores (Table 3) generated the highest hydrocarbon selectivity (41.4 area %), which was 66% times higher than that in the blank experiment (25.0 area%). Increased hydrocarbon selectivity is associated with decreased oxygenate selectivity, and the oxygenate types are notably dependent on the different porous materials. The SBA-15 catalyst favored the conversion of aldehydes/acids into hydrocarbons, whereas MCM-41 and large-pore zeolites (Beta and Y) led to a greater reduction in phenols and ketones. Because the latter molecules are more stubborn than acids or aldehydes, the decreased phenol/ketone selectivity confirmed the higher deoxygenation activity for the large-pore zeolites (Beta and Y) [49]. The weak acidity of MCM-41 indicated a poor deoxygenation capability, and its mesopores resulted in the repolymerization of phenols to coke, which is consistent with its high solid yield (Fig. 4**a**).

The gas composition exhibited a similar variation when porous materials were applied as the first-layered catalysts. Compared to the blank experiment, all the porous materials increased the total volumetric percentage of CO_2 and CO at the expense of decreasing that for H_2 and CH_4. This suggests that in addition to dehydration, the oxygen in biomass vapors was mainly removed through decarboxylation and decarbonylation reactions, consistent with the carbonium ion mechanism occurring at the zeolite acidic sites during biomass CFP [50]. Interestingly, the Beta zeolite exhibited the highest fraction of CO_2 and CO (90.9 vol%), indicating its highest deoxygenation capability.

In summary, porous materials are suitable candidates for first-layered catalysts with the aim of producing hydrocarbon-rich bio-oil. In particular, the addition of mesoporous SBA-15 led to a barely-reduced bio-oil yield with a satisfactory hydrocarbon selectivity, and the addition of Beta zeolite provided the most-deoxygenated bio-oil among all the investigated first-layered catalysts.

3.3. *Comparative performance of all the first-layered catalyst types*

As shown in Fig. 5, the bio-oil yield obtained from each dual-catalyst CFP test was plotted against its hydrocarbon selectivity. The corresponding data for the blank experiment (*Thermal/ZSM-5*) are highlighted as the reference point, which exhibits a value of 19.4 wt% (bio-oil yield) and 25.0 area% (hydrocarbon selectivity). The bio-oil yield was reduced for all the investigated first-layer catalysts. This was as expected, because the removal of oxygen from primary volatiles induces a carbon rearrangement in the three (gas, liquid, and solid) and the formation of water, which subsequently reduced the liquid and bio-oil yields [41]. The bio-oil yield reduction trend for the first-layered catalyst types was inorganic salts > metal oxides > porous materials. The mesoporous silica SBA-15 barely reduced the bio-oil yield (19.4 wt %). This is attributed to the adsorption and stabilization of the active oxygenated intermediates within their porosity, which prevents their repolymerization to coke [47]. The deoxygenation degree is also dependent on the first-layered catalysts, and thus most acidic catalysts (*e.g.*, $MgCl_2$, Al_2O_3, Beta zeolite, and Y zeolite) increased the hydrocarbon selectivity, which is probably related to the favored dehydration route. For all first-layered catalysts, their deoxygenation capability was enhanced in the order of porous materials > inorganic salts > metal oxides. The Beta zeolite exhibited the best performance in deoxygenating bio-oils and demonstrated the highest hydrocarbon selectivity (41.4 area%). This is consistent with previous reports that most deoxygenation reactions occur at the Brönsted acidic sites inside zeolite channels [51]. The diagram in Fig. 5 allows for a rapid evaluation of the catalytic performance of all first-layered catalysts in terms of both bio-oil yield and hydrocarbon selectivity. The dual-catalyst combinations located on the upper right of the diagram are evidently superior to those located on the lower left. For example, the combination of first-layered catalysts of Y zeolite, SBA-15, or K_2HPO_4 with ZSM-5 yielded a high hydrocarbon selectivity (27.7–31.3 area%) and a satisfactory bio-oil yield (18.5–19.4 wt%). In addition, the porous materials generally performed better than other catalyst types (inorganic salts and metal oxides) in synergy with ZSM-5 by producing the most deoxygenated bio-oil with an adequate yield.

Given that the pore sizes of SBA-15, Y, and Beta zeolites are larger than that of ZSM-5, the combination of the first-layered (SBA-15, Y, or Beta zeolite) and second-layered catalyst (ZSM-5) can be viewed as a "hierarchical zeolite catalyst" in a whole. This type of "composite catalyst" functionalizes more like a core–shell catalyst; that is, the mesopores/large-pores of first-layered catalysts (*e.g.*, SBA-15, Y, Beta zeolites) cracked the heavy oxygenates in biomass vapors to lighter ones,

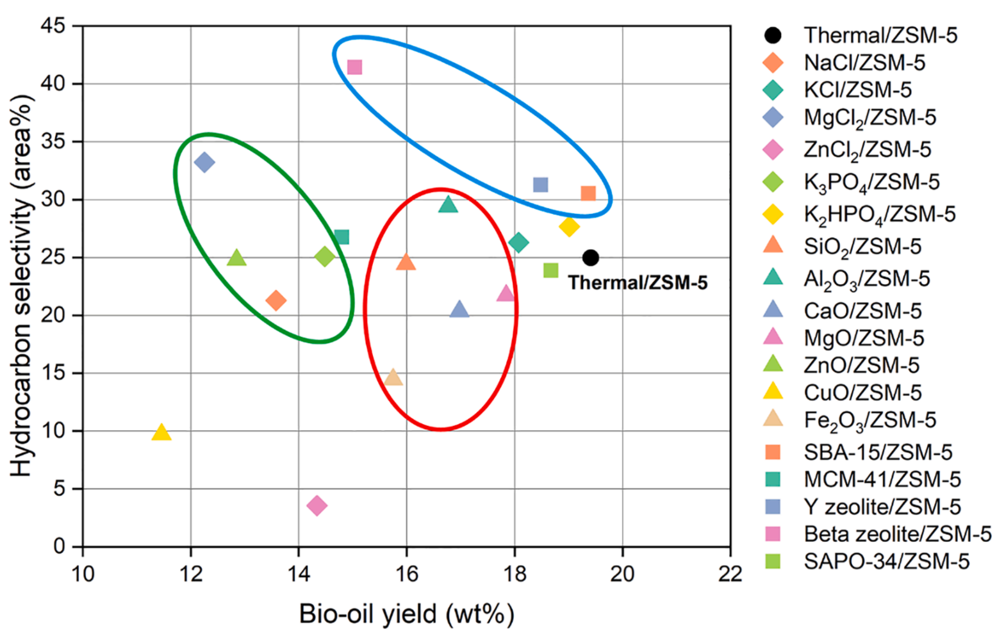

Fig. 5. The comparative catalytic activity of all the first-layered catalysts in combination with ZSM-5. The inorganic salts, metal oxides, and porous materials are circled in green, red, and blue, respectively.

and the acid sites inside the medium-sized pores of ZSM-5 further deoxygenated the light oxygenates to aromatic hydrocarbons. Owing to the complicated synthetic methods used to prepare core–shell catalysts, the dual-catalyst combination used in this work is a convenient alternative to improve the bio-oil quality of biomass CFP.

3.4. Comparative study on the single- and double-catalysts CFP

To gain deeper insight into the dual-catalyst CFP technology, the single-catalyst mode using six inorganic salts (NaCl, KCl, $MgCl_2$, $ZnCl_2$, K_3PO_4, and K_2HPO_4), seven metal oxides (SiO_2, Al_2O_3, CaO, MgO, ZnO, Fe_2O_3, and CuO), and five porous materials (SBA-15, MCM-41, Y, Beta, and SAPO-34) were also conducted, and the results are summarized in **Fig. S10–S12** in the Supporting Information. Compared to the non-catalytic pyrolysis of poplar sawdust (denoted as *Thermal*), the single-catalyst mode tends to produce a slightly reduced bio-oil yield with an extremely low hydrocarbon selectivity (0–4.0 area%). Although these single catalysts are not suitable for deoxygenizing primary volatiles, they help to reduce the complexity of bio-oil by enriching certain compounds. This phenomenon is more evident for inorganic-salt catalysts. For example, the $ZnCl_2$ or $MgCl_2$ catalysts sharply reduced the number of detected species in bio-oil from 50, for non-catalytic pyrolysis, to 17–20. The resulting bio-oil was mainly composed of furfural ($ZnCl_2$: 67.4 area%; $MgCl_2$: 43.3 area%) and acetic acid ($ZnCl_2$: 24.8 area%; $MgCl_2$: 30.7 area%) (**Fig. S10b**). Similarly, the K_3PO_4 catalyst led to a bio-oil consisting mainly of phenols (61.0 area%) and ketones (24.1 area%) (**Fig. S10b**). The upgraded bio-oil was accompanied by a varied gas composition. In particular, $MgCl_2$ increased the fraction of CO_2 from 46.5 to 64.2 vol%, whereas $ZnCl_2$ and K_3PO_4 increased the H_2 fraction from 4.3 to 31.0 and 12.4 vol%, respectively (Table S2). Therefore, the quality of the biomass volatiles was improved after upgrading with first-layered catalysts.

The addition of a second-layered catalyst (ZSM-5) notably boosted the production of hydrocarbons, which is attributed to the effective deoxygenating capability of ZSM-5. However, it is noted that the deoxygenated species and deoxygenation degree varied with the first-layered catalysts. For a better illustration, the chemical selectivity variation impacted by ZSM-5 was recorded for all the first-layered catalysts (Fig. 6). The hydrocarbon selectivity evidently increased in all cases. Regarding the oxygenates, the ketone selectivity declined more than the other oxygenate types (acids, aldehydes, and phenols) when metal oxides and porous materials were applied as first-layered catalysts, which was accompanied by enhanced CO production (Table 4). This is attributed to a higher ketone percentage in biomass volatiles after upgrading with first-layered catalysts; on the other hand, this is caused by enhanced aldol condensation and aromatization reactions for ketones (*e.g.*, acetones) over ZSM-5. The decrease in ketone selectivity was even larger for acidic metal oxides (*e.g.*, MgO, ZnO, Al_2O_3), suggesting a stronger deoxygenation activity of ZSM-5 for ketones in these cases. For the first-layered catalysts of inorganic salts, the oxygenate variation imparted by ZSM-5 is related to the acid-base properties of inorganic salts. That is, for neutral salts (KCl and NaCl) and basic salts (K_2HPO_4 and K_3PO_4), the selectivity reduction of ketones and phenols was larger than that of acids and aldehydes. This also increased the selectivity for H_2 and CH_4 except for NaCl. However, for acidic salts ($ZnCl_2$ and $MgCl_2$), the aldehyde selectivity decreased to a greater extent, owing to the larger furfural fraction in the pre-upgraded biomass vapors. As mentioned above, the cracking efficiency of ZSM-5 is dependent on the first-layered catalyst type, and a synergistic effect exists between the layered catalysts.

To illustrate the synergistic effect more clearly, Fig. 7 plots the reduction in oxygenate selectivity as a function of the hydrocarbon selectivity increase for all the dual-catalyst combinations. Interestingly,

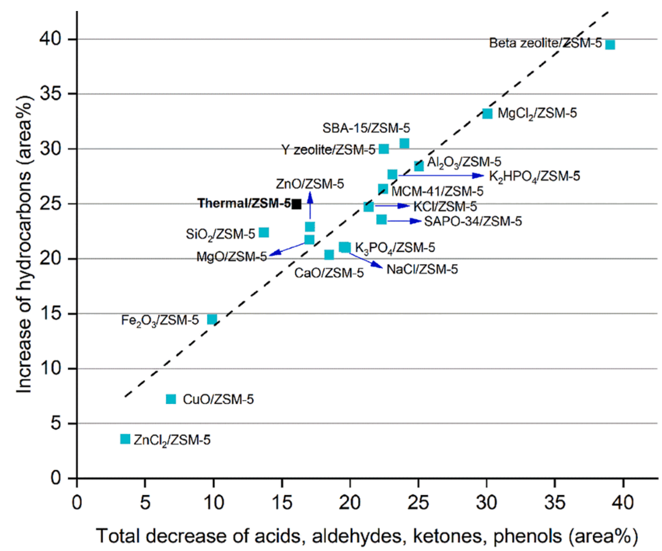

Fig. 7. The selectivity reduction of oxygenates as a function of the selectivity increase of hydrocarbons over all the catalyst combinations.

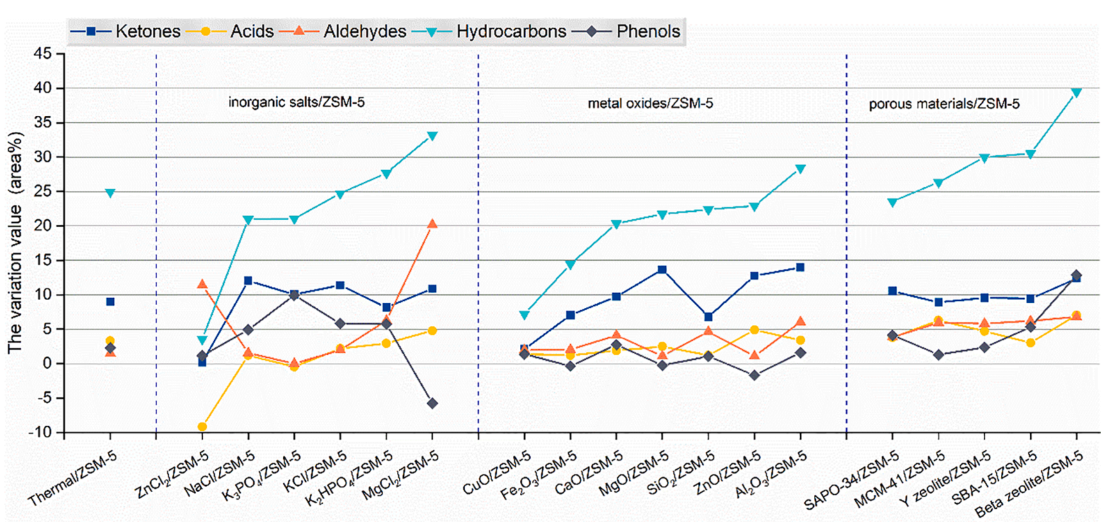

Fig. 6. Chemical selectivity variation impacted by the secondary ZSM-5 catalyst for all the first-layered catalysts. Note: the ordinate represents the increase of hydrocarbons and reduction of ketones, acids, aldehydes, and phenols.

the overall variation trend was graphically linear. Taking the corresponding data of *Thermal/ZSM-5* as a reference, the dual-catalyst combinations in the upper right part of the curve are characterized by a higher conversion of oxygenates to hydrocarbons, which indicates a better synergistic effect between the first-layered catalyst (*e.g.*, Beta zeolite and $MgCl_2$) and secondary ZSM-5. In particular, the catalyst layout of Beta + ZSM-5 exhibited the highest value by converting 39.0 area% oxygenations to 41.4 area% hydrocarbons. This is confirmed by the previous results showing that the addition of Beta zeolite strengthened the cracking efficiency of ZSM-5 in all oxygenate types (ketones, phenols, acids, and aldehydes) (Fig. 6). In contrast, the dual-catalyst combinations (*e.g.*, $ZnCl_2$ + ZSM-5, CuO + ZSM-5, Fe_2O_3 + ZSM-5) located on the lower left of the plot exhibited a lower oxygenate conversion rate, suggesting a poor synergistic effect between these layered catalysts. The $ZnCl_2$ + ZSM-5 combination exhibited the lowest synergistic effect, although the deoxygenation activity of ZSM-5 for furfural was enhanced. From the diagram, the catalyst layout of Beta + ZSM-5 is recommended for enhancing hydrocarbon production in the dual-catalyst CFP of poplar sawdust.

4. Conclusions

A systematic study of the dual-catalyst CFP of poplar sawdust was conducted using 18 first-layered catalysts (six inorganic salts, seven metal oxides, and five porous materials) in combination with a fixed second-layer catalyst (ZSM-5). The effects of the different first-layered catalysts on bio-oil production were investigated and compared. Compared to inorganic salts and metal oxides, the application of porous materials as first-layered catalysts yielded a superior deoxygenated bio-oil with a satisfactory yield. This catalyst also exhibited a positive synergistic effect with the secondary ZSM-5 catalyst. Among all the catalyst combinations, SBA-15 + ZSM-5 produced the highest bio-oil yield (19.4 wt%), whereas Beta + ZSM-5 yielded a bio-oil with the highest hydrocarbons selectivity (41.4 area%).

Declaration of Competing Interest

The authors declare that they have no known competing financial interests or personal relationships that could have appeared to influence the work reported in this paper.

Acknowledgements

This work was supported by the National Natural Science Foundation of China (21906005, 22176009), Beijing Natural Science Foundation (8194068), and the PetroChina Innovation Foundation. The authors thank Zhengzhou University for assistance with the equipment. Dr. J. Liang also thanks the financial support from Beihang University.

Appendix A. Supplementary data

Supplementary data to this article can be found online at https://doi.org/10.1016/j.cej.2021.134251.

References

[1] V. Samburova, J. Connolly, M. Gyawali, R.L. Yatavelli, A.C. Watts, R. K. Chakrabarty, B. Zielinska, H. Moosmüller, A. Khlystov, Polycyclic aromatic hydrocarbons in biomass-burning emissions and their contribution to light absorption and aerosol toxicity, Sci. Total Environ. 568 (2016) 391–401.
[2] J.M. Bergthorson, M.J. Thomson, A review of the combustion and emissions properties of advanced transportation biofuels and their impact on existing and future engines, Renew. Sust. Energ. Rev. 42 (2015) 1393–1417.
[3] S. Wang, G. Dai, H. Yang, Z. Luo, Lignocellulosic biomass pyrolysis mechanism: a state-of-the-art review, Prog. Energy Combust. Sci. 62 (2017) 33–86.
[4] X. Chen, Q. Che, S. Li, Z. Liu, H. Yang, Y. Chen, X. Wang, J. Shao, H. Chen, Recent developments in lignocellulosic biomass catalytic fast pyrolysis: Strategies for the optimization of bio-oil quality and yield, Fuel Process. Technol. 196 (2019), 106180.
[5] H. Zhang, R. Xiao, B. Jin, G. Xiao, R. Chen, Biomass catalytic pyrolysis to produce olefins and aromatics with a physically mixed catalyst, Bioresour. Technol. 140 (2013) 256–262.
[6] Q. Che, M. Yang, X. Wang, X. Chen, W. Chen, Q. Yang, H. Yang, H. Chen, Aromatics production with metal oxides and ZSM-5 as catalysts in catalytic pyrolysis of wood sawdust, Fuel Process. Technol. 188 (2019) 146–152.
[7] X. Xue, Z. Pan, C. Zhang, D. Wang, Y. Xie, R. Zhang, Segmented catalytic co-pyrolysis of biomass and high-density polyethylene for aromatics production with $MgCl_2$ and HZSM-5, J. Anal. Appl. Pyrol. 134 (2018) 209–217.
[8] S. Leng, X. Wang, J. Wang, Y.e. Liu, F. Ma, X. Zhong, Waste tire pyrolysis for the production of light hydrocarbons over layered catalysts, Energy Technol. 3 (2015) 851–855.
[9] H. Zhang, J. Zheng, R. Xiao, Y. Jia, D. Shen, B. Jin, G. Xiao, Study on pyrolysis of pine sawdust with solid base and acid mixed catalysts by thermogravimetry–fourier transform infrared spectroscopy and pyrolysis–gas chromatography/mass spectrometry, Energy Fuels. 28 (2014) 4294–4299.
[10] S. Liu, Q. Xie, B. Zhang, Y. Cheng, Y. Liu, P. Chen, R. Ruan, Fast microwave-assisted catalytic co-pyrolysis of corn stover and scum for bio-oil production with CaO and HZSM-5 as the catalyst, Bioresour. Technol. 204 (2016) 164–170.
[11] B. Zhang, Z. Zhong, P. Chen, R. Ruan, Microwave-assisted catalytic fast co-pyrolysis of Ageratina adenophora and kerogen with CaO and ZSM-5, J. Anal. Appl. Pyrol. 127 (2017) 246–257.
[12] S. Wang, Z. Li, X. Bai, W. Yi, P. Fu, Catalytic pyrolysis of lignin in a cascade dual-catalyst system of modified red mud and HZSM-5 for aromatic hydrocarbon production, Bioresour. Technol. 278 (2019) 66–72.
[13] H. Zhang, P.K.W. Likun, R. Xiao, Improving the hydrocarbon production via co-pyrolysis of bagasse with bio-plastic and dual-catalysts layout, Sci. Total Environ. 618 (2018) 151–156.
[14] D. Ro, Y.M. Kim, I.G. Lee, J. Jae, S.C. Jung, S.C. Kim, Y.K. Park, Bench scale catalytic fast pyrolysis of empty fruit bunches over low cost catalysts and HZSM-5 using a fixed bed reactor, J. Clean Prod. 176 (2018) 298–303.
[15] C. Liu, H. Wang, A.M. Karim, J. Sun, Y. Wang, Catalytic fast pyrolysis of lignocellulosic biomass, Chem. Soc. Rev. 43 (2014) 7594–7623.
[16] N. Zhao, B.X. Li, The effect of sodium chloride on the pyrolysis of rice husk, Appl. Energy 178 (2016) 346–352.
[17] C. Branca, C. Di Blasi, A. Galgano, Catalyst screening for the production of furfural from corncob pyrolysis, Energy Fuels 26 (2012) 1520–1530.
[18] Q. Lu, C.Q. Dong, X.M. Zhang, H.Y. Tian, Y.P. Yang, X.F. Zhu, Selective fast pyrolysis of biomass impregnated with $ZnCl_2$ to produce furfural: Analytical Py-GC/MS study, J. Anal. Appl. Pyrol. 90 (2011) 204–212.
[19] Z.B. Zhang, Q. Lu, X.N. Ye, L.-P. Xiao, C.Q. Dong, Y.Q. Liu, Selective production of phenolic-rich bio-oil from catalytic fast pyrolysis of biomass: Comparison of K_3PO_4, K_2HPO_4, and KH_2PO_4, BioResources 9 (2014) 4050–4062.
[20] A. Eschenbacher, A. Saraeian, P.A. Jensen, B.H. Shanks, C. Li, J.Ø. Duus, T.E. L. Smitshuysen, C.D. Damsgaard, A.B. Hansen, K.I. Kling, Deoxygenation of wheat straw fast pyrolysis vapors over $Na\text{-}Al_2O_3$ catalyst for production of bio-oil with low acidity, Chem. Eng. J. 394 (2020), 124878.
[21] S.D. Stefanidis, S.A. Karakoulia, K.G. Kalogiannis, E.F. Iliopoulou, A. Delimitis, H. Yiannoulakis, T. Zampetakis, A.A. Lappas, K.S. Triantafyllidis, Natural magnesium oxide (MgO) catalysts: a cost-effective sustainable alternative to acid zeolites for the in situ upgrading of biomass fast pyrolysis oil, Appl. Catal. B-Environ. 196 (2016) 155–173.
[22] C. Torri, M. Reinikainen, C. Lindfors, D. Fabbri, A. Oasmaa, E. Kuoppala, Investigation on catalytic pyrolysis of pine sawdust: Catalyst screening by Py-GC-MIP-AED, J. Anal. Appl. Pyrol. 88 (2010) 7–13.
[23] J. Liang, G. Shan, Y. Sun, Catalytic fast pyrolysis of lignocellulosic biomass: Critical role of zeolite catalysts, Renew. Sust. Energ. Rev. 139 (2021), 110707.
[24] E. Iliopoulou, E. Antonakou, S. Karakoulia, I. Vasalos, A. Lappas, K. Triantafyllidis, Catalytic conversion of biomass pyrolysis products by mesoporous materials: effect of steam stability and acidity of Al-MCM-41 catalysts, Chem. Eng. J. 134 (2007) 51–57.
[25] J.W. Kim, S.H. Joo, B. Seo, S.S. Kim, D.H. Shin, S.H. Park, J.K. Jeon, Y.K. Park, Bio-oil upgrading via catalytic pyrolysis of waste mandarin residue over SBA-15 catalysts, J. Nanosci. Nanotechnol. 13 (2013) 2566–2572.
[26] R. Liu, M. Sarker, M.M. Rahman, C. Li, M. Chai, R. Cotillon, N.R. Scott, Multi-scale complexities of solid acid catalysts in the catalytic fast pyrolysis of biomass for bio-oil production–A review, Prog. Energy Combust. Sci. 80 (2020), 100852.
[27] J. Jae, G.A. Tompsett, A.J. Foster, K.D. Hammond, S.M. Auerbach, R.F. Lobo, G. W. Huber, Investigation into the shape selectivity of zeolite catalysts for biomass conversion, J. Catal. 279 (2011) 257–268.
[28] Y. Wang, L. Ke, Y. Peng, Q. Yang, Y. Liu, Q. Wu, Y. Tang, H. Zhu, L. Dai, Z. Zeng, Ex-situ catalytic fast pyrolysis of soapstock for aromatic oil over microwave-driven HZSM-5@ SiC ceramic foam, Chem. Eng. J. 402 (2020), 126239.
[29] K. Cai, S. Huang, Y. Li, Z. Cheng, J. Lv, X. Ma, Influence of acid strength on the reactivity of dimethyl ether carbonylation over H-MOR, ACS Sustainable Chem. Eng. 7 (2019) 2027–2034.
[30] M. Su, R. Yang, M. Li, Biodiesel production from hempseed oil using alkaline earth metal oxides supporting copper oxide as bi-functional catalysts for transesterification and selective hydrogenation, Fuel 103 (2013) 398–407.
[31] B. Xaba, A. Mahomed, H. Friedrich, The effect of CO_2 and H_2 adsorption strength and capacity on the performance of Ga and Zr modified Cu-Zn catalysts for CO_2 hydrogenation to methanol, J. Environ. Chem. Eng. 9 (2021), 104834.
[32] S. Ma, S. Chen, A. Soomro, M. Zhu, W. Xiang, Characterization of Fe_2O_3/CeO_2 oxygen carriers for chemical looping hydrogen generation, Int. J. Hydrogen Energy 43 (2018) 3154–3164.

[33] D. Wang, L. Jin, Y. Li, B. Wei, D. Yao, H. Hu, Effect of reducibility of transition metal oxides on in-situ oxidative catalytic cracking of tar, Energy Convers. Manage. 197 (2019), 111871.
[34] C.D. Blasi, C. Branca, A. Galgano, Products and global weight loss rates of wood decomposition catalyzed by zinc chloride, Energy Fuels 22 (2008) 663–670.
[35] Z. Cao, J. Niu, Y. Gu, R. Zhang, Y. Liu, L. Luo, Catalytic pyrolysis of rice straw: Screening of various metal salts, metal basic oxide, acidic metal oxide and zeolite catalyst on products yield and characterization, J. Clean Prod. 269 (2020), 122079.
[36] H. Yang, R. Yan, H. Chen, D. Lee, C. Zheng, Characteristics of hemicellulose, cellulose and lignin pyrolysis, Fuel 86 (2007) 1781–1788.
[37] K. Ding, Z. Zhong, J. Wang, B. Zhang, L. Fan, S. Liu, Y. Wang, Y. Liu, D. Zhong, P. Chen, Improving hydrocarbon yield from catalytic fast co-pyrolysis of hemicellulose and plastic in the dual-catalyst bed of CaO and HZSM-5, Bioresour. Technol. 261 (2018) 86–92.
[38] S.D. Stefanidis, K.G. Kalogiannis, E. Iliopoulou, A. Lappas, P. Pilavachi, In-situ upgrading of biomass pyrolysis vapors: catalyst screening on a fixed bed reactor, Bioresour. Technol. 102 (2011) 8261–8267.
[39] J. Shao, R. Yan, H. Chen, H. Yang, D.H. Lee, Catalytic effect of metal oxides on pyrolysis of sewage sludge, Fuel Process. Technol. 91 (2010) 1113–1118.
[40] A.G. Gayubo, A.T. Aguayo, A. Atutxa, R. Aguado, M. Olazar, J. Bilbao, Transformation of oxygenate components of biomass pyrolysis oil on a HZSM-5 zeolite. II. Aldehydes, ketones, and acids, Ind. Eng. Chem. Res. 43 (2004) 2619–2626.
[41] C. Zhang, L. Zhang, Q. Li, Y. Wang, Q. Liu, T. Wei, D. Dong, S. Salavati, M. Gholizadeh, X. Hu, Catalytic pyrolysis of poplar wood over transition metal oxides: Correlation of catalytic behaviors with physiochemical properties of the oxides, Biomass Bioenergy 124 (2019) 125–141.
[42] Y. Shao, X. Hu, Z. Zhang, K. Sun, G. Gao, T. Wei, S. Zhang, S. Hu, J. Xiang, Y. Wang, Direct conversion of furfural to levulinic acid/ester in dimethoxymethane: Understanding the mechanism for polymerization, Green, Energy Environ. 4 (2019) 400–413.
[43] S. Ratchahat, S. Kodama, W. Tanthapanichakoon, H. Sekiguchi, CO_2 gasification of biomass wastes enhanced by Ni/Al_2O_3 catalyst in molten eutectic carbonate salt, Int. J. Hydrogen Energy 40 (2015) 11809–11822.
[44] H. Ding, Y. Xu, C. Luo, Q. Wang, C. Shen, J. Xu, L. Zhang, A novel composite perovskite-based material for chemical-looping steam methane reforming to hydrogen and syngas, Energy Convers. Manage. 171 (2018) 12–19.
[45] K. Otsuka, Y. Wang, E. Sunada, I. Yamanaka, Direct partial oxidation of methane to synthesis gas by cerium oxide, J. Catal. 175 (1998) 152–160.
[46] M.A. Uddin, H. Tsuda, S. Wu, E. Sasaoka, Catalytic decomposition of biomass tars with iron oxide catalysts, Fuel 87 (2008) 451–459.
[47] Z. Ma, E. Troussard, J.A. van Bokhoven, Controlling the selectivity to chemicals from lignin via catalytic fast pyrolysis, Appl. Catal. A-Gen. 423 (2012) 130–136.
[48] Y. Zhao, L. Deng, B. Liao, Y. Fu, Q.X. Guo, Aromatics production via catalytic pyrolysis of pyrolytic lignins from bio-oil, Energy Fuels 24 (2010) 5735–5740.
[49] A.G. Gayubo, A.T. Aguayo, A. Atutxa, R. Aguado, J. Bilbao, Transformation of oxygenate components of biomass pyrolysis oil on a HZSM-5 zeolite. I. Alcohols and phenols, Ind. Eng. Chem. Res. 43 (2004) 2610–2618.
[50] D.J. Mihalcik, C.A. Mullen, A.A.J.J.o.A. Boateng, A. Pyrolysis, Screening acidic zeolites for catalytic fast pyrolysis of biomass and its components, J. Anal. Appl. Pyrol. 92 (2011) 224–232.
[51] T.R. Carlson, G.A. Tompsett, W.C. Conner, G.W. Huber, Aromatic production from catalytic fast pyrolysis of biomass-derived feedstocks, Top. Catal. 52 (2009) 241–252.